An enquiry into theoretical bioinorganic chemistry: How heuristic is the character of present-day quantum chemical methods?

Maren Podewitz, Martin T. Stiebritz and Markus Reiher*

Received 12th March 2010, Accepted 10th May 2010
DOI: 10.1039/c004195e

In this discussion we elaborate on the state of the art in computational bioinorganic chemistry and aim at identifying and defining the most difficult obstacles in the process of obtaining unambiguous and predictive results from quantum chemical calculations. We then proceed to discuss and analyse well-known as well as new concepts for overcoming some of these obstacles.

1 Introduction

Bioinorganic chemistry is a very complex and diverse field. Structures with different types of ligands ranging from chelate co-factors to full proteins, with a varying number of interacting (transition) metals provide the stage for the most complex chemical transformations and for intricate reaction mechanisms: prominent examples are the dioxygen evolution at the water-oxidizing complex of Photosystem II[1–3] or reductions at the active centers of Hydrogenases[4,5] or Nitrogenases.[6] From the perspective of active sites, the protein environment represents a coordination sphere of utmost complexity.

The optimum way to understand the function of such systems is to accomplish a perfect structural and time resolution of their catalytic chemical reactions to obtain results that explain experimental studies but also to provide complementary information not accessible in experiment. Exactly this is at least in principle possible by a quantum mechanical description based on the elementary particles of chemistry, *i.e.*, the electrons and the atomic nuclei.[7] However, the mono- and polynuclear transition-metal active sites demand highly accurate electronic structure methods. These have to be very flexible with respect to the type of electron correlation to be described because of the diverse bond-breaking and bond-formation processes that can occur—apart from the high density of states that emerges from open-shell transition-metal centers and unsaturated ligands.

Reliability and predictability of calculations on such systems depend crucially on the accuracy of these necessarily approximate electronic structure methods. Unfortunately, to date there still does not exist a universal and well-established computational protocol for the study of bioinorganic reaction mechanisms in proteins and enzymes. Instead, recipes have been established by various schools which are not always congruent with one another and which feature a somewhat heuristic character. This is because of the method-inherent errors and because of the large set of parameters to cope with in an electronic structure method—for example: structural model, spin state, charge, solvation, choice of the density functional (in Density Functional Theory (DFT)) *etc*.

Laboratorium für Physikalische Chemie, ETH ZurichWolfgang-Pauli-Strasse 10, 8093 Zurich, Switzerland. E-mail: markus.reiher@phys.chem.ethz.ch

One aim of theoretical bioinorganic chemistry—despite the elucidation of the structural and functional variety of a particular system—should be to develop universally valid concepts that allow us to extract chemical principles from the calculated results unaffected by method-inherent errors. These concepts must be transferable to different systems beyond the consideration of individual case studies.

In this paper we will elaborate on some thoughts along these lines and begin with three theses on the computational modeling of bioinorganic reaction sites in order to stimulate a discussion on the future progress and options of theoretical bioinorganic chemistry beyond the mere accurate calculation of specific experimental results for a particular metalloenzyme. In order to illustrate these three theses, we will discuss two concepts to address structure and reactivity of a model active site, focus on structure–property correlations, and investigate the flexibility of transition states.

2 Three theses on the current status of computational bioinorganic chemistry

Quantum mechanics applied to chemistry, *i.e.*, quantum chemistry, allows us to study the electrons (and atomic nuclei) within the stationary picture of the time-independent electronic Schrödinger equation,

$$\hat{H}_{el}\Psi_{el,n} = E_{el,n}\Psi_{el,n} \quad (1)$$

which assigns a nuclear-coordinate-dependent electronic energy $E_{el,n}$—the so-called potential energy hypersurface—to a collection of electrons and nuclei in electronic state *n via* application of the electronic Hamiltonian operator $\hat{H}_{el}$ to the many-electron wave function $\Psi_{el,n}$ (after having introduced the convenient Born–Oppenheimer approximation). Molecular structures of educts, products, reactive intermediates, and transition states are stationary points on this surface $E_{el,n}$, which also directly provides their relative energies (at 0 K without zero-point vibrational effects). Molecular properties of these structures that may eventually allow one to identify them by experiment are obtained from $E_{el,n}$ by differentiation with respect to external perturbations like electromagnetic fields.[8–10]

Quantum chemistry meets its greatest challenges in the description of metalloproteins because of the size of these molecules and the fact that the correlated motion of the electrons is particularly difficult to capture in an ansatz for the many-electron wave function. Electron correlation is an issue for large conjugated ligands (like porphyrins), soft ligand atoms (like sulfur atoms), open-shell transition metals (like iron or manganese), which all come together to provide the stage for the chemistry enabled by metalloproteins. Of course, these challenges are not specific to computational bioinorganic chemistry, but to computational chemistry in general albeit they are most prominent in the field of bioinorganic chemistry.

2.1 Thesis 1: Method-inherent approximations are difficult to control

Approximations are inevitable for the solution of eqn (1). It is important to separate unnecessary approximations from the most crucial ones. Purely technical issues like effective core potentials, approximate relativistic Hamiltonians and one-electron basis sets[11] can be well controlled. By contrast, the most crucial approximations which we have to control very carefully (at least we must pursue to do so) are those that affect the description of electron correlation. In DFT this is the choice of the exchange–correlation energy density functional, while it is the choice of the many-electron basis in case of a wavefunction-based *ab initio* method.

Mathematically speaking, the electronic wave function can be exactly expanded into a complete basis of many-electron functions (or somewhat less rigorous: of electronic configurations),

$$\Psi_{el,n} = \sum_{i_1 i_2 \cdots i_N} C^{(n)}_{i_1 i_2 \cdots i_N} \quad |i_1 i_2 \cdots i_N\rangle \tag{2}$$

which is called full configuration interaction (F-CI). Wavefunction-based *ab initio* methods now try to approximate this expansion by selecting a *finite* number of configurations $|i_1 i_2 \cdots i_N\rangle$. Prominent examples of these attempts are truncated CI expansions, coupled-cluster approaches or multiconfiguration methods like the complete-active-space self-consistent field (CASSCF) method.[12] However, all these methods implicitly assume that the construction scheme for the many-electron basis set is so general that it can cope with any chemical situation. The assumption is especially challenged in reactions of transition-metal clusters that break more than one bond at a time.

Ab initio methods are universal and systematically improvable in principle, but for a specific structure under consideration it is often not clear how fast convergence with increasing size of the many-electron basis set is. Convergence can be slow for active sites of interest to bioinorganic chemistry and the limited capabilities of highly accurate *ab initio* methods may prohibit arrival at truly converged results. Even worse, the accuracy of such methods changes with position on the potential energy hypersurface so that the effect on relative energies like reaction energies or barrier heights can be difficult to control and to predict. Systematic improvability can hence become a myth when improvement of the many-electron basis is not significant if only deadwood is picked up in Hilbert space.

Consequently, computational bioinorganic chemistry requires truly universal methods which yield a constant error at any point of the potential energy hypersurface $E_{el,n}$, but there exists so far no completely satisfying solution to this problem in the standard repertoire. In recent work, we pursued a different strategy and adopted novel concepts developed in physics for model Hamiltonians like the Heisenberg or the Hubbard Hamiltonian.[13,14] The principle idea is not to generate a pre-defined many-electron basis set but to construct directly the most important CI coefficients and to leave it to the algorithm to determine the electronic configurations that feature CI coefficients above a certain threshold. One such method is the density matrix renormalization group algorithm (DMRG),[15–17] which constructs CI coefficients from so-called matrix product states (MPS)[18,19]

$$\Psi^{\mathrm{MPS}}_{el} = \sum_{i_1 i_2 \cdots i_N} A^{[1]}_{i_1} A^{[2]}_{i_2} \cdots A^{[N]}_{i_N} \quad |\, i_1 i_2 \cdots i_N\rangle \tag{3}$$

where the transformation matrices $A^{[k]}_{i_k}$ represent the change of the basis when adding to systematically constructed many-particle states on an active subset of orbitals explicitly described states on an additional orbital taken from the complementary subset (note that $A^{[1]}_{i_1}$ and $A^{[N]}_{i_N}$ are vectors). However, also such an ansatz has its drawbacks and calculations on transition metal complexes are not trivial even if they are feasible[13] (also for DMRG the increase of DMRG basis states to improve the accuracy represents a major bottleneck and leads to highly sophisticated calculations that cannot be carried out routinely on a daily or weekly basis[20]). Still, novel *ab initio* methods are being developed. For instance, a new type of parametrization are the so-called tensor network states.[21–23] Such an ansatz was for the first time considered for a full quantum chemical Hamiltonian $\hat{H}_{el}$ by Marti *et al.*[14]

For our pioneering DMRG study on transition metal clusters[13] we selected the $Cu_2O_2^{2+}$ core of copper containing enzymes that has been identified by Cramer and collaborators[24] as a particularly difficult case for electronic structure methods. Cramer *et al.* plotted the relative energy for the interconversion of bis(μ-oxo) and the side-on peroxo structures of $Cu_2O_2^{2+}$ along a one-dimensional isomerization path for various quantum chemical methods. While all methods deviate from one another at some distance, the failure of CASSCF is particularly striking indicating the decisive role of a sufficiently large active orbital space that allows one to construct an at least qualitatively correct many-electron wave function.

Perturbation-theory calculations of second order (CAS-PT2) on top of such a result are then not able to cure the qualitatively wrong behaviour of the CASSCF wave function. This difficulty of the CASSCF/CASPT2 approach has attracted some attention.[25,26]

Of course, the most popular method in computational bioinorganic chemistry is DFT—because of the feasibility of such calculations rather than because of their reliability. In principle, there exists an exact energy density functional that allows us to calculate the potential energy surface $E_{el,0}$ of the electronic ground state from the electronic density alone owing to the first Hohenberg–Kohn theorem.[27] However, we only know approximations to this functional which we assume to be more accurate the more advanced the terms considered are, in the sense of a Jacob's ladder,[28] but increased accuracy is not guaranteed.

The approximate density functionals are not systematically improvable and hence if a failure is somehow detected, it cannot be cured. Usually, density functionals are judged on the basis of a statistical analysis of results obtained for a test set of molecules. Very many such studies exist and can thus hardly be reviewed here. The problem is that such stochastic statements on the accuracy of density functionals depend on the choice of test molecules and quantities in the training set. In a particular case under consideration one can hardly tell the accuracy of the results obtained. Method-inherent discrepancies are regularly observed when studying transition metal complexes and clusters with DFT. To provide an example from our own work we refer to the binding energy of dinitrogen to the central iron atom of Sellmann-type model complexes designed as biomimetic models to mimic nitrogen fixation. Here, we observed discrepancies between the BP86 and B3LYP density functionals of about 70 kJ mol^{-1}.[29] In such cases, one may choose the worst case result in order to still draw a chemically relevant conclusion.

Interestingly, although relative electronic energies may differ largely from functional to functional, it is often claimed (also by us) that certain quantities like molecular structures or properties can be reproduced quite reliably with some established functionals. This, however, is a matter of experience gained by studying very many examples. For more rigorous evidence of this belief one would have to show that derivatives of the electronic energy are predicted more accurately than relative electronic energies.

Actually, the situation is even worse. The accuracy of DFT methods (and others are not even feasible for this purpose) is not sufficient to predict a structure of an active site in a metalloenzyme. On the contrary, DFT calculations can only be performed on the mode of action of a metalloenzyme once the molecular structure of its active site has been resolved experimentally. A prominent example is the recently discovered central ligand in the FeMo-cofactor of nitrogenase[30] that had been neglected in first DFT calculations that nevertheless 'explained' the mechanism. However, it is important to understand that such studies on wrong sites or faulty active-site structures are still very useful because also the wrong mechanisms that seemed to be plausible at first sight point to a deeper understanding of the true mode of action once this is known.

2.2 Thesis 2: Structural models of active sites are not easy to construct

The errors introduced into the potential energy surface due to the method-inherent approximations in chemical methods are not the only sources of uncertainties that could corrupt a scientific conclusion on the chemical reactivity and molecular properties of a metalloenzyme's active site. Eqn (1) is to be solved for a predefined molecular structure and hence a structural model has to be chosen for modeling the chemical behavior of the active site. One may argue that the complete enzyme structure—taken, for instance, from an X-ray diffraction experiment—should provide a good starting point. However, eqn (1) can be solved for a molecular structure of about 200 atoms rather than for a structure of more than 2,000 atoms let

alone 200,000 atoms. Therefore, small structural models of the metal cluster and its surrounding ligand sphere that carefully resemble the active site structure within the protein need to be chosen. This also includes the selection of solvent molecules considered to be relevant. However, choices made at this stage will certainly lead to deviations from the true structural behaviour of the metalloprotein.

Fortunately, reaction energetics are dominated by the ligand binding energies to the active site and usually dominate by far all other interaction energies (although this is not always guaranteed, of course, and dynamic effects come into play when ligand binding energies are small and of the order of strong hydrogen bond energies). This is the reason why we can expect that structural models of restricted size may well represent the essential chemistry the active site is capable of performing.

Of course, advanced methods that include the complete protein environment are available. Most prominent are the so-called QM/MM methods (see ref. [31] for a most recent review). Here, however, the protein environment is modelled by a collection of classical charges parametrized to reproduce certain protein properties. Invoking a QM/MM model provides the comfy feeling that the complete metalloprotein is considered at the cost of new additional approximations (classical-mechanical energy contribution evaluated for a parametrized force-field that electrostatically interacts with the quantum-mechanical kernel where the reactions take place).

2.3 Thesis 3: Transferable results are difficult to extract

Even if the two major obstacles of computational modeling in bioinorganic chemistry could be satisfactorily solved (Theses 1 and 2), we would obtain for a given system one particular number for the quantity under consideration. It was Max Planck who once said: 'Wenn man genau ermittelt hat, wieviele Körner irgendein Sandhaufen enthält, so ist das eine ungeheure Leistung. Aber man kann mit dieser Zahl nichts weiter anfangen, weil sie nur eine ganz spezielle Bedeutung besitzt'[32] (*Translation*: *If one has determined the exact number of grains in some pile of sand, then this is a huge accomplishment. However, one cannot benefit from this number because it has only very special meaning*.) The true challenge in science is to put these numbers into context in order to extract principles that govern chemical reactivity and that eventually allow us to design synthetic (biomimetic) catalysts which can accomplish the function for which nature invented metalloenzymes. Only if transferable knowledge is provided can we expect to rationally re-design metalloenzymes for other purposes than those of the wild-type enzymes and also to design new biomimetic systems. Hence, the question arises what are the proper theoretical and computational means to do that so that we do not end up collecting unrelated numerical data?

3 Correlation diagrams for quantitative structure–property relations

For transition metal chemistry, the equilibrium structure of the (catalytically active) transition metal core is determined by the ligand sphere and by the environment in general, which mutually influence the electronic structure, *i.e.*, the oxidation state, the spin distribution, and the charge distribution. In addition to these system-inherent structural variations, we have to deal with the method-inherent variations: optimized stationary structures may vary for different quantum chemical methods.

Being able to estimate the method-inherent errors and the system-inherent variations is a mandatory step en route to understanding transition-metal chemistry and to develop unifying and system-transgressing concepts. In order to gain insight into the nature (properties) and reactivity of such transition-metal clusters, we may investigate the flexibility of these clusters in terms of correlation diagrams. These diagrams have a long history and were particularly popular in times when

computational resources and algorithms had not been developed yet (*e.g.*, Walsh diagrams, Tanabe–Sugano or Orgel diagrams). The potential energy hypersurface provides a direct means to correlate structures to each other if screened properly in the space of relevant coordinates.

However, we are not only interested in the variance in energy of an active site with respect to nuclear positions but also in the change of its molecular properties with respect to cluster structure. Relevant properties are, *e.g.*, the total electronic spin expectation value and the spin density distribution that can be assigned to atomic centers by local spin expectation values.[33–37] Local spin values denote the excess of α- or β-electrons on a certain atom or a group of atoms.[33] For this purpose, the molecule can be divided into local basins defined by atom-centered basis functions such that projection operators allow us to decompose the total spin expectation value $\langle \hat{S}^2 \rangle$ or its projection onto the z-axis $\langle \hat{S}_z \rangle$.[33–36]

Following the example already discussed, we investigate the structural flexibility of transition-metal clusters at the example of the planar dinuclear copper model cluster $[Cu_2O_2]^{2+}$ with respect to the different spin states, total charges, and density functionals by continuously screening relevant cluster structures. Such copper-cluster structures are central moieties in active sites of various enzymes in nature. Activation of dioxygen is mediated by copper-containing proteins like oxyhemocyanin or oxytyrosinase[38,39] (see also for dicopper–oxygen complexes refs. [40–43]). Cramer *et al.*[24] investigated the structural changes from the bis(μ-oxo) to the side-on peroxo structure. However, this scan was only one-dimensional. Here, we present a two-dimensional scan of the Cu–Cu and the O–O bond lengths as well as a scan of the properties such as the total and the local spin expectation values. Apart from insights into the electronic structure of the cluster, representations of local spin properties depending on the cluster structure allow us also to identify whether the wave function has converged always to the same electronic configuration or whether different structures yield qualitatively different Kohn–Sham determinants with distinct molecular properties, such as local spin distributions. This, of course, also allows us to detect whether the energy and property scans are without technical flaws that may arise because of convergence to local energy minima in parameter space of MO coefficients. Qualitative changes in electronic structure are thus easily identified and can be substantiated or eliminated by convergence control.[37,44]

3.1 Technical issues

In order to arrive at a detailed picture of the structural flexibility of the system, it is necessary to scan higher-dimensional potential energy and property surfaces of which certain cuts can be conveniently plotted. In the current illustrative example, we shall restrict ourselves to the two structural degrees of freedom that emerge when the $[Cu_2O_2]^{2+}$ cluster is distorted within the plane of all nuclei. Thus, we shall present here such a two-dimensional scan of the Cu–Cu and the O–O bond lengths as well as of total and local spin expectation values.

A graphical representation of the scanned $[Cu_2O_2]$ structures is depicted in Fig. 1. Our scan includes the bis(μ-oxo) and the side-on peroxo structures studied by Cramer *et al.*[24] We investigated three different spin states: the high-spin $S = 2$ state, the triplet $S = 1$ state, and the $S = 0 \rightarrow M_S = 0$ broken-symmetry (BS) state with the BP86, B3LYP, and TPSS density functionals.

For each scan we chose a step size of 0.26 Å for the Cu–Cu bond and of 0.13 Å for the O–O bond resulting in 242 grid points of the potential energy surface. As initial-guess molecular orbitals the converged α- and β-molecular orbitals (MOs) of the bis(μ-oxo) structure were provided. For further details of the potential energy surface and property surface generation, the reader is referred to the "Computational Methodology" section in the appendix. The potential energy surface plots are presented in Fig. 2, where the structure with the lowest energy has been arbitrarily set equal to zero and all structures up to a relative energy of 1000 kJ mol^{-1}

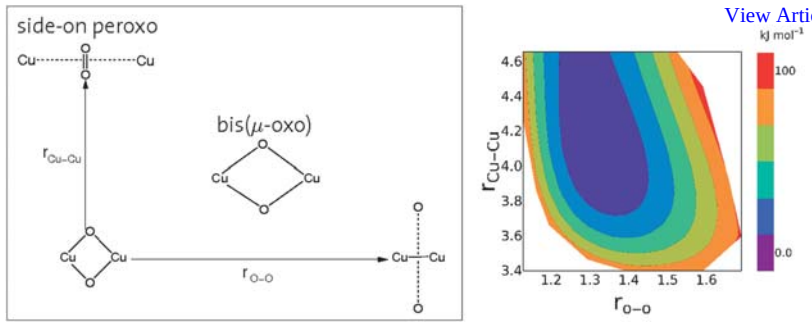

Fig. 1 Graphical illustration of the $[Cu_2O_2]$ structure scan (left): from left to right the O–O bond length is scanned from 1.0 Å to 3.8 Å, whereas from bottom to top the Cu–Cu bond length is plotted from 2.0 Å to 4.7 Å. A cut through the potential energy hypersurface around the most stable side-on peroxo TPSS/RI/TZVP-optimized triplet structure displays the smooth potential well (right).

are depicted. For each scan, all other structures with a higher relative energy than 1000 kJ mol^{-1}, which may occur due to unfavorable electron–electron and nucleus–nucleus repulsion at short distances, were omitted. The overall picture of the potential energy surface is little affected by this choice of maximum energy plotted as can be seen from the plot of the potential energy hypersurface around the most stable TPSS/RI/TZVP optimized $[Cu_2O_2]$ triplet structure presented on the right hand side of Fig. 1 when compared with the same plot in Fig. 2 (middle). It can be seen that the potential energy well is smooth around the most stable structure, when relative energies up to 100 kJ mol^{-1} are plotted.

From Fig. 2 it can be seen that the structural flexibility of the $[Cu_2O_2]^{2+}$ cluster depends on the spin state (and somewhat on the density functional employed). Although all density functionals predict a bis(μ-oxo) structure to be most stable for the high-spin state, the TPSS and the B3LYP functionals show a second local energy minimum for the side-on peroxo structure. In case of B3LYP the bis(μ-oxo) and the side-on peroxo structure are separated by a barrier.

Interestingly, in the TPSS/triplet structure a distinct area with higher stability compared to the surrounding points is visible for an O–O separation of about 3.0 Å and a Cu–Cu distance between 3.6 and 4.6 Å. Analysis of the total spin expectation value $\langle \hat{S}^2 \rangle$ and the local spin expectation value on the Cu center shows cusps in the property surface as witnessed in the middle panel of Fig. 2 (see below). Closer inspection reveals that this higher stability may arise due to convergence of the initial guess orbitals to local-minimum solutions, which are identical to the converged orbitals at the equilibrium structure. One might also attribute this to our current resolution of the potential-energy-surface grid but test calculations with a smaller step size yield very similar results. Thus, the impact of the initial guess MOs on the potential energy hypersurface is more pronounced than the influence of grid resolution: all characteristics of the potential energy hypersurface for the fine grid are already visible for the hypersurfaces at lower resolution. Hence, one is alarmed by those individual cases where the surface is not smooth but features kinks that may arise due to an improper choice of the initial guess MOs.

As a first conclusion, we understand that such automatically performed potential energy scans provide very useful information that may prevent one from drawing incorrect conclusions based on technical deficiencies (approximate density functional or orbital convergence to local energy minima) or from exaggerating individual numerical results. The value of such plots can therefore hardly be overestimated. One may argue that the single-point calculations may become unfeasible for larger clusters or small clusters with large ligand environments (large cofactor ligands or fragments of the protein environment). However, present-day DFT

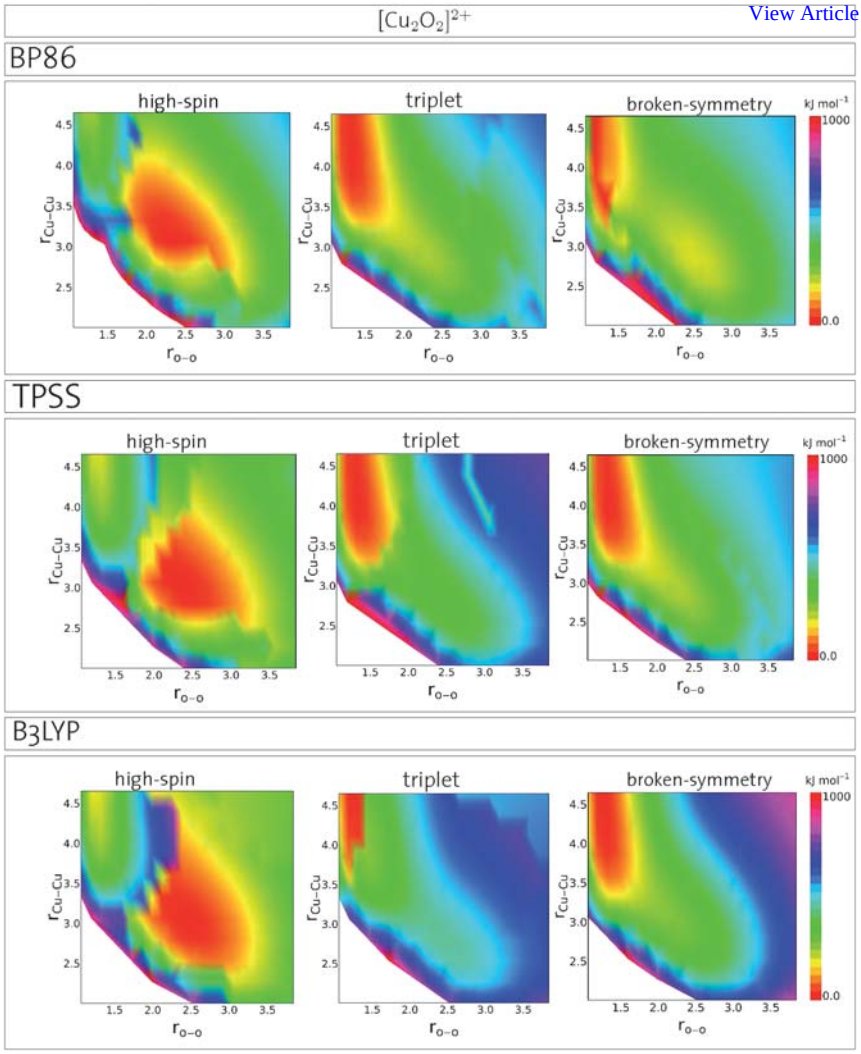

Fig. 2 Potential energy plots for the $[Cu_2O_2]^{2+}$ cluster in high-spin, triplet and broken-symmetry states as obtained with the BP86, B3LYP, and the TPSS density functionals.

programs are remarkably efficient and a set of single-point calculations can easily be carried out in parallel on widely available computer clusters. Finally, if the reliability of results and chemical conclusions can be increased, limited computer time must not be an objection.

3.2 Relating results for specific choices of charge and ligand environment

In the following we shall delve somewhat deeper into the information that can be extracted from correlation diagrams.

The equilibrium structure for a given spin state also depends on the overall charge of the cluster, which can be seen in Fig. 3, where the potential energy surface plots of the $M_S = 0$ broken-symmetry state are depicted for three different total charges of the cluster: $[Cu_2O_2]^{2-}$, $[Cu_2O_2]^{0}$, and $[Cu_2O_2]^{2+}$. The electron rich clusters $[Cu_2O_2]^{2-}$ and $[Cu_2O_2]^{0}$ favor the bis(μ-oxo) structure, whereas for $[Cu_2O_2]^{2+}$ the side-on peroxo structure is most stable.

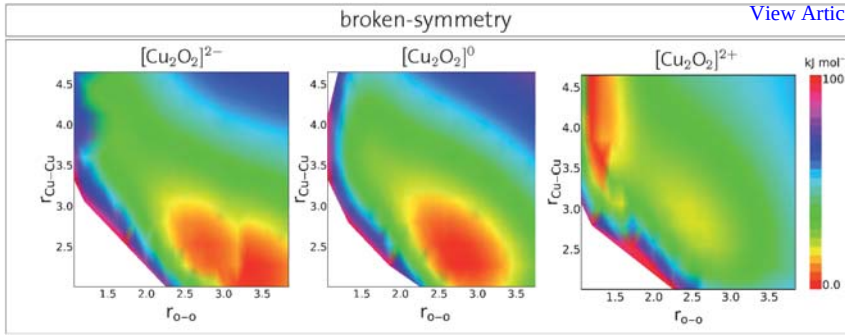

Fig. 3 Comparison of the BP86/RI/TZVP potential energy plots for the broken-symmetry state of differently charged clusters $[Cu_2O_2]^{2-}$, $[Cu_2O_2]^{0}$, and $[Cu_2O_2]^{2+}$.

From these results we observe a certain flexibility of the investigated clusters and get an estimate for the depth of the potential well, which depends on the individual spin state, total charge, and the density functional employed. Still, we only studied the generic $[Cu_2O_2]$ cluster structure and the flexibility is, of course, modified by a ligand sphere that may stabilize a bis(μ-oxo), a side-on peroxo, or any other type of O_2 coordination (*cf.* ref. [45]).

An example that highlights the effect of ligands on the generic correlation plots is presented in Fig. 4. Here, we compare the triplet state potential energy hypersurface of the generic $[Cu_2O_2]$ cluster (left) with that of the $[Cu_2O_2(NH_3)_2]^{2+}$ cluster (right), where the copper centers are embedded in a square-planar ligand field generated by four NH_3 ligands and the two μ-oxo bridges. It can be seen that for the $[Cu_2O_2(NH_3)_2]^{2+}$ cluster both a side-on and a bis(μ-oxo) species are stable with the bis(μ-oxo) structure being energetically slightly favored, whereas for the generic $[Cu_2O_2]^{2+}$ complex only a side-on peroxo species is stable. The ligand sphere can, however, be modeled by point charges of −0.75 a.u. at the positions of the nitrogen atoms as can be seen from Fig. 4 (middle). The point charges do not only shift the stability of the generic cluster towards the bis(μ-oxo) structure but also reproduce the potential energy hypersurface of the full-fledged cluster. Thus, such a simplified model can mimic the reactivity of the full-fledged cluster. The electrostatic embedding can therefore conveniently be employed for the generation of a structural model abstracted from a specific ligand sphere.

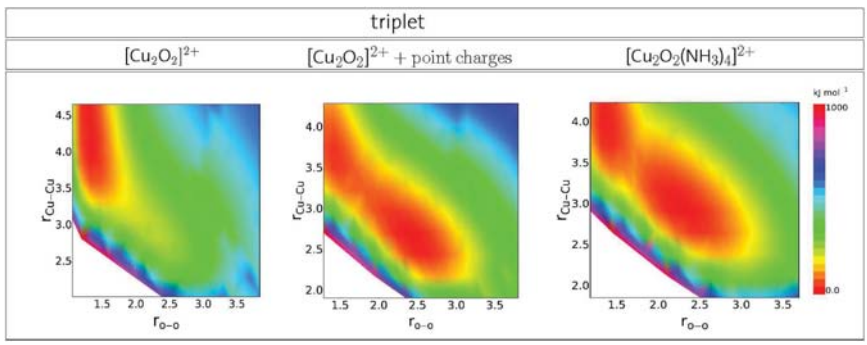

Fig. 4 Comparison of the BP86/RI/TZVP potential energy surfaces for the triplet state of the generic $[Cu_2O_2]^{2+}$ complex (left), the $[Cu_2O_2(NH_3)_2]^{2+}$ cluster (right) and the generic $[Cu_2O_2]^{2+}$ cluster with ligands substituted by point charges (middle). The ammonia ligand sphere promotes a bis(μ-oxo) structure and point charges of −0.75 a.u. mimic this electronic effect.

3.3 Comparison of two $[Cu_2O_2]^{2+}$ broken-symmetry states

For the broken-symmetry state of $[Cu_2O_2]^{2+}$ two different local spin distributions could be converged: the BS1 state, where the two copper atoms are coupled ferromagnetically, and the BS2 state, where the Cu centers couple in an antiferromagnetic fashion. These two different local spin distributions correspond to two different Slater determinants yielding two different potential energy surfaces as is evident from Fig. 5.

The qualitative electronic difference between the two broken-symmetry states becomes further evident when comparing the local $\langle \hat{S}_{zA} \rangle$ spin expectation values depicted in Fig. 6. The BS1 state features ferromagnetic coupling of the two copper centers, where on each metal atom the local spin value is larger than zero indicating an excess of α-spin, whereas both oxygen atoms carry a negative local spin referring to an excess in β-spin except for the region with large Cu–Cu and O–O bond lengths. Here, the oxygen atoms couple in an antiferromagnetic fashion with local spin values of about -0.8 and 0.8 a.u., respectively. The local spin plots of the BS2 state, however, clearly indicate an antiferromagnetic coupling of the Cu atoms, where each metal center carries a local spin but with inverted sign. Absolute local spin values on the metal centers are approximately the same for the BS1 and the BS2 state. By analysis of these property plots, we can conclude that BS1 exhibits a symmetric local spin distribution with respect to the metal atoms—both metal atoms carry a local spin of the same value and sign. Furthermore, it is clear from Fig. 5 and 6 that the most stable side-on peroxo structure is in fact a closed-shell structure because local spin values are smaller than 0.0001 a.u., while the bis(μ-oxo) structure shows antiferromagnetically coupled copper atoms.

Although the two different electronic structures represented by two different Kohn–Sham Slater determinants feature a side-on peroxo structure to be most stable, the relative energy difference between these two Slater determinants varies from -150.0 kJ mol^{-1} in favor of the BS1 state up to 300 kJ mol^{-1} in favor of the BS2 state. The relative energy differences between the two BS states were obtained by subtraction of the total energies of the two states at each grid point. In the region of the side-on peroxo coordination the BS1 state is lower in energy, whereas in the region of the bis(μ-oxo) structure the BS2 state is energetically favored. The plot illustrates that the type of magnetic coupling can also depend on the structural parameters such as metal–metal and oxygen–oxygen bond lengths.

Although for this small generic $[Cu_2O_2]^{2+}$ cluster both Slater determinants favor the side-on peroxo coordination of O_2, a ligand sphere may alter this situation and stabilize a bis(μ-oxo) structure or a structure, where the energy difference between these two states is negligible. Given a ligand sphere stabilizes a structure in which the energy difference between the two broken-symmetry states is small

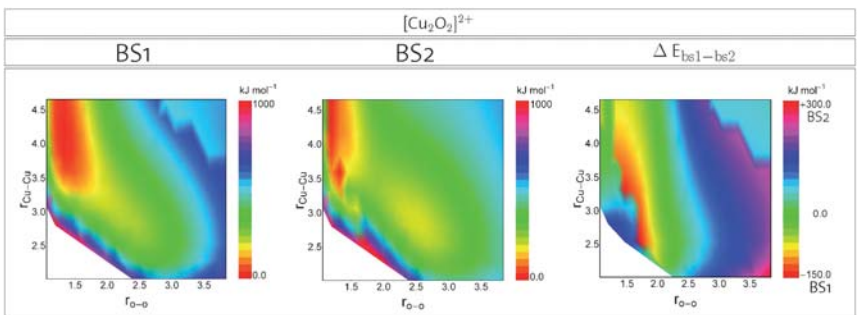

Fig. 5 The two BP86/RI/TZVP potential energy surfaces of the BS1 and the BS2 broken-symmetry states of $[Cu_2O_2]^{2+}$ as well as the relative energy difference between the two potential hypersurfaces. Bond lengths are given in Å.

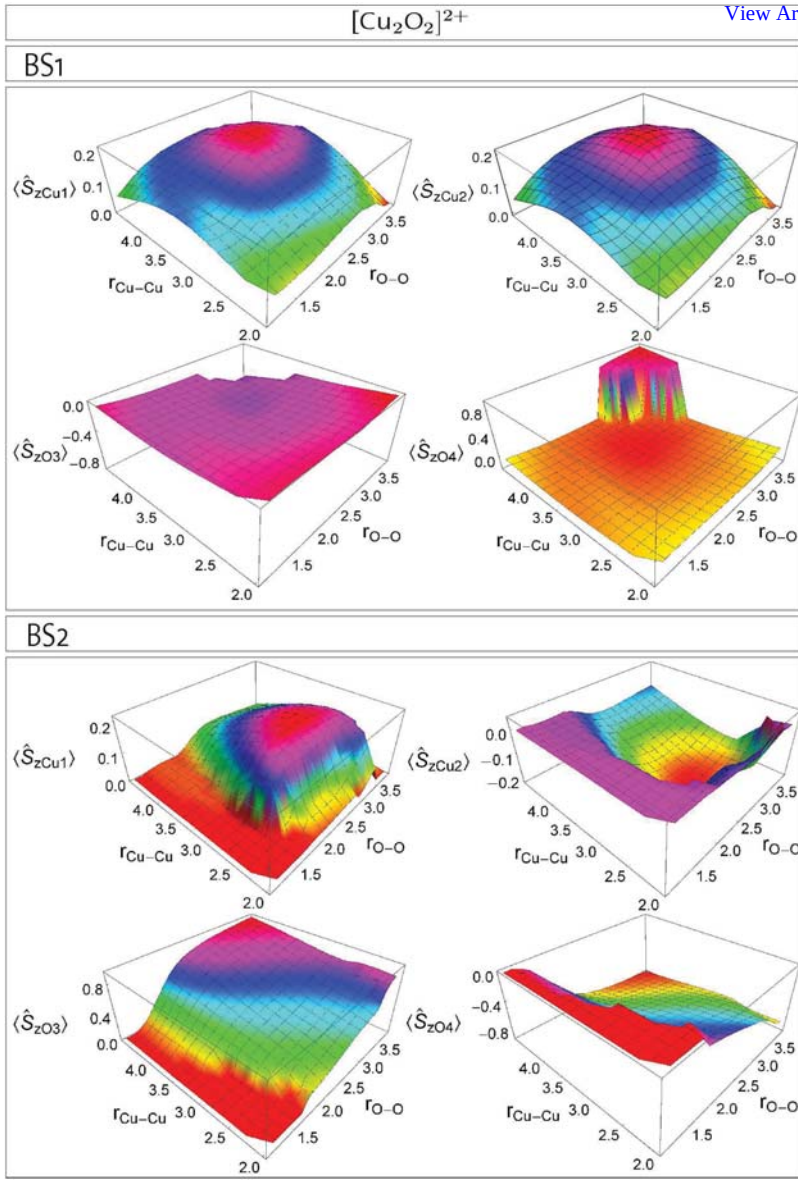

Fig. 6 Comparison of local $\langle \hat{S}_{zA} \rangle$ spin expectation values calculated for all atoms A for the two different broken-symmetry states of $[Cu_2O_2]^{2+}$.

compared to the method-inherent error of the quantum chemical protocol employed, it is not only impossible to predict which state is more stable, but also the two potential energy surfaces may intersect. Hence, the cluster may switch between the two states during a reaction and one must be aware of this in quantum chemical modeling. (Note that we are well aware of the model character of a broken-symmetry state in DFT when compared to a rigorous description by an *ab initio* method.[46]) This behavior is conceptually different from a well known singlet–triplet crossing because the molecular broken-symmetry spin state is maintained, only local properties change. Here, one may object that all these problems vanish if an appropriate quantum chemical method—like a reliable multireference *ab initio* method—replaces

the DFT approach. That is often, however, a mere assumption neglecting the facts that feasibility usually prevents the use of high-accuracy quantum chemical approaches and that the quality of their results is also not constant for different structures on the potential energy surface due to the finite many-electron basis set as discussed above.

While we have analyzed the potential energy surfaces and the local spin plots, we shall now relate them to the total spin expectation values $\langle \hat{S}^2 \rangle$ as depicted in Fig. 7.

We observe that the onset of local spins on the oxygen atoms for the BS1 state is accompanied by an increase of the total $\langle \hat{S}^2 \rangle$ expectation, that in turn is a measure for the spin contamination of the cluster structures. This effect is even more pronounced for the BS2 state. In both cases, it can be seen that the increase in spin contamination correlates with the onset of increased local spin distribution on the atoms, *i.e.*, with the transition from a closed-shell state with no α- or β-spin excess to an open-shell species, where spin pairing is no longer perfectly obeyed.

4 Chemical reactivity and transition state flexibility

The reliable prediction of chemical reactivity and revealing possible reaction paths is a central capability of quantum chemical approaches. In order to draw any reliable conclusion from calculations of reaction energies or barrier heights it is a prerequisite to understand the impact of the method-inherent error on the particular molecular system under study. Whereas the calculation of stationary points on the potential energy hypersurface, required *e.g.*, for the calculation of binding energies, is generally considered to be straightforward, the question of accuracy is more severe for the calculation of rate constants where deviations in barrier heights on the order of 10 kJ mol^{-1} already produce an error in the rate constant of more than one order of magnitude. Moreover, because usually transition-state structures are obtained under idealized conditions—*i.e.*, by simplifying or neglecting the influence of the surrounding like the protein environment—it is necessary to estimate how, in general, barrier heights are affected by small distortions of the molecular geometry.

In order to verify that a calculated structure represents a proper transition state one performs a vibrational analysis that should then reveal only one normal mode with imaginary frequency. Additionally to this information the procedure provides a complete set of normal modes that can be considered as basis vectors for constructing any allowed movement of the molecular architecture within the harmonic approximation.

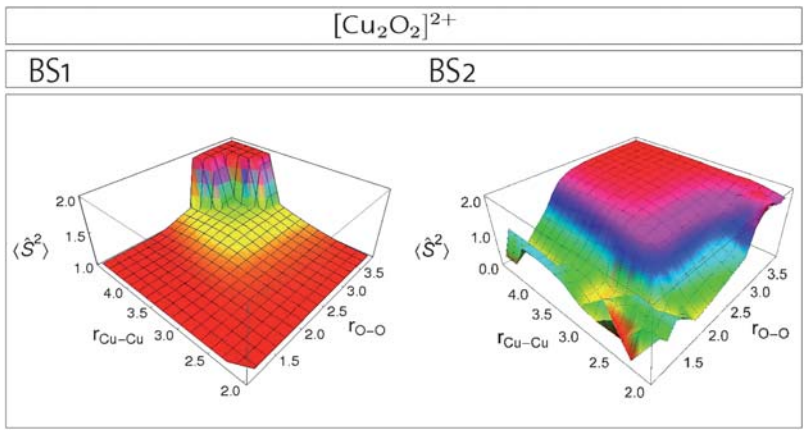

Fig. 7 Comparison of total spin expectation values $\langle \hat{S}^2 \rangle$ for the two broken-symmetry states of $[Cu_2O_2]^{2+}$ BS1 and BS2.

In order to grasp the flexibility of a transition-state structure we now consider its distortion in such a way that a given energy threshold shall not be exceeded. When studying the active site of a metalloenzyme (or of any synthetic catalyst in general) this corresponds to the question to what extent the structure can vary from the ideal one at the rate-determining first-order saddle point of the potential energy surface without sacrificing the activity of the catalyst.

In our approach here, we consider distortions along low-frequency normal modes that describe activity-related vibrations. These vibrations are those that affect the ligand to metal center distances and orientations rather than intra-ligand vibrations which are not likely to play a role for the reaction mechanism. Of course, within the harmonic approximation of the potential energy surface around the saddle point, we may directly relate the increase in energy to the distortion along a normal mode,

$$E_{\mathrm{pot},i} = \frac{1}{2} Q_i^{(m)\dagger} F_{ii}^{(m)} Q_i^{(m)} \tag{4}$$

if we adopt a semi-classical picture that neglects the quantization of the nuclear motion. With $Q_i^{(m)}$ denoting the ith mass-weighted normal mode and F_{ii} representing the corresponding force constant, *i.e.*, the ith element of the diagonalized mass-weighted Hessian, which can be reformulated in terms of the wavenumber $\tilde{\nu}_\mathrm{i}$ of the ith normal mode by using,

$$\tilde{\nu}_i = \frac{1}{\lambda_i} = \frac{1}{2\pi c}\sqrt{F_{ii}^{(m)}} \tag{5}$$

to arrive at

$$E_{\mathrm{pot},i} = E_{\mathrm{cutoff}} = 2\pi^2 c^2 \tilde{\nu}_i Q_i^{(m)^2} \tag{6}$$

As an example for illustrating the transition-state-flexibility concept we choose a model structure by Hall and co-workers[47] which resembles a transition state in the reaction mechanism of the iron-containing enzyme methylenetetrahydromethanopterin dehydrogenase (Hmd) that catalyzes the reversible oxidation of molecular hydrogen. The reaction mechanism of the active site was studied with DFT by Yang and Hall and we consider here a transition state $\mathbf{TS}_{2,3}$,[47] that is passed upon splitting the bond of a dihydrogen molecule bound to the central iron atom to yield two hydrogen atoms attached to the metal and to the sulfur atom of a coordinating cysteine residue (see Fig. 8).

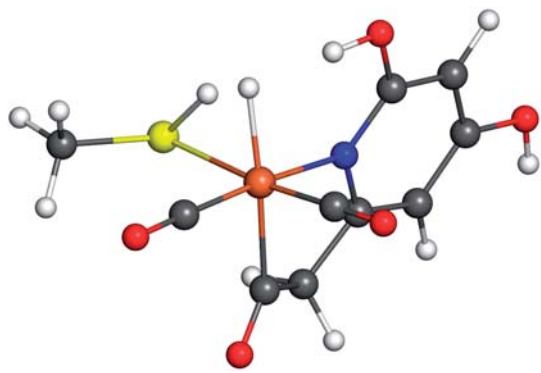

Fig. 8 Transition state $\mathbf{TS}_{2,3}$ of methylenetetrahydromethanopterin dehydrogenase (Hmd) from the work of Yang and Hall.[47] One of the hydrogen atoms is still attached to the central iron atom whereas the other is already connected to the sulfur atom of a coordinating cysteine residue (modeled as thiomethanolate). Element coloring scheme: White = H, red = 0, blue = N, grey = C, yellow = S, brown = Fe.

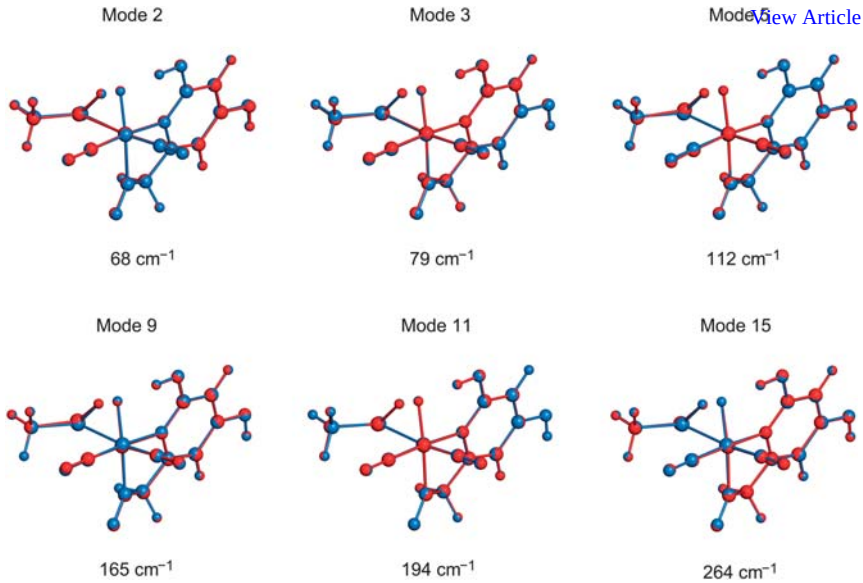

Fig. 9 Distortion of the transition state $\mathbf{TS}_{2,3}$ from ref. 47 along selected normal modes. The distortions were generated such as to not exceed an energy increase by about 10 kJ mol^{-1}. The figure shows superpositions of the perturbed structures (red) with the true transition state structure (blue) and lists the corresponding wavenumber $\tilde{\nu}_i$ for each node.

After performing a vibrational analysis, the transition state was distorted along selected normal modes without exceeding an increase in energy by more than approx. 10 kJ mol^{-1} per mode. For the selection we focused on low-frequency modes that should allow a significant molecular distortion and which should involve the thiomethanolate group with which the metal cluster is attached to the protein, because this position allows a direct influence by the protein environment. As the superpositions of the resulting structures with the optimized transition-state structure of $\mathbf{TS}_{2,3}$ demonstrate (Fig. 9) the geometrical variations needed to reach this threshold are very subtle.

Note that such results have implications for the computational design of catalysts, as, *e.g.*, for the design of enyzme active sites, where single optimized transition-state structures of model active sites are used as a guide to properly arrange/design the protein environment for catalysis,[48,49] because our data show that even small distortions have the potential to significantly impede reactivity.

5 Conclusions

In this Faraday discussion paper, we pursued the stimulation of a discussion on the reliability and validity of quantum chemical methods in bioinorganic chemistry that may reach beyond the mere calculation of individual numerical results for specific active sites. While feasibility has been a big issue in the past, modern algorithms and implementations in combination with the efficiency of comparatively cheap computer clusters puts us in a position where the question of reliability becomes of utmost importance. Once this is solved, we are still left with the question of how to design a most appropriate model system for the study of the active site in a metalloprotein. Finally, the question arises of how to extract system transgressing results on the chemistry of a particular transformation from the quantitative data provided by quantum chemical calculations.

While we have reviewed some material from the literature to substantiate the first two theses, we argued in favor of two concepts to tackle the third thesis. First we presented a plea for the use of correlation diagrams to relate energies and properties

of relevant cluster structures. The relevance of a certain cluster structure is, of course, determined by the chemistry that is performed by this cluster, which also conveniently reduces the coordinate space to be investigated in correlation diagrams. For our generic dinuclear copper model cluster we encountered diverse technical and reliability problems that would hardly be evident in standard calculations that focus solely on individual optimized stationary points with predefined spin and charge. Hence, correlation diagrams provide a means to identify such problems and prevent one from overinterpreting the calculated data. Electrostatic embedding of the generic cluster accounts for electronic effects of a specific ligand sphere and can be employed as a simplified surrogate system.

Moreover, the correlation diagrams allow us to grasp the flexibility of a cluster structure by investigation of relevant sections of the potential energy hypersurface. In this sense, they help us to understand the structural flexibility and with some imagination also the dynamics of the cluster that could otherwise only be extracted by involved (first-principles) molecular dynamics simulations. The diagrams also aid us in relating different structural and electronic features of the cluster under consideration. It is obvious that one may plot many useful properties in such diagrams that allow one to better understand its reactivity. It is even possible to probe the coordination energy of a ligand at the different structures spanned by the correlation plot.

The second concept proposed the flexibility of transition state structures. Here, the standard procedure is to optimize a single transition state structure and to assign an energy for the barrier height. This barrier height, however, does depend on the structural model that is chosen (apart from the fact that it also depends on the accuracy of the quantum chemical method selected) and it is not clear from inspection of the single structure how flexible or rigid that structure is with respect to distortions that may lead to an increase in electronic energy. The concept of normal-mode guided perturbation can be employed as a valuable tool to estimate the range of structural flexibility of a given transition state in order to assess whether the structural distortion is still consistent with energetic boundary conditions required by the catalytic cycle under consideration as, for instance, highlighted in the kinetic model by Kozuch and Shaik.[50,51]

The examples discussed in this paper were designed to demonstrate that a broader perspective in quantum chemical studies of reaction mechanisms in bioinorganic chemistry is suitable to arrive at a more complete and reliable picture of the active site's reactivity.

Computational methodology

All-electron calculations were carried out with the DFT programs provided by the TURBOMOLE suite.[52] The complexes and clusters were treated as open-shell systems in the unrestricted Kohn–Sham framework. The self-consistent-field (SCF) single point calculations were considered to be converged when the energy difference between two cycles was less than 10^{-6} Hartree. For all atoms included in our complex and cluster models we used Ahlrichs' valence triple-ζ TZVP basis set with polarization functions[53] on all atoms.

For the calculations we used different density functionals, namely the Becke–Perdew exchange–correlation functional dubbed BP86,[54,55] the hybrid B3LYP functional,[56,57] and the TPSS functional[28] (for the non-hybrid functionals, BP86 and TPSS, we invoked the resolution-of-the-identity (RI) approximation as implemented in TURBOMOLE). We chose those functionals for the correlation diagrams to get an estimate for the functional-inherent discrepancies—especially for the differences between the pure and the hybrid density functionals—and thus, extend the results from the study of Cramer *et al.*[24] They found that the pure density functionals, such as TPSS, BLYP, and mPWPW91, predict the relative energy gap of the bis(μ-oxo) and the side-on peroxo $[Cu_2O_2]^{2+}$ more accurately than the hybrid density

functionals compared to the completely renormalized coupled-cluster CR-CCD(T) and CR-CCSD/TQ) benchmark calculations.

The structure–property plots were obtained by a two-dimensional scan of the metal–metal and O–O bond lengths. For each structure (grid point) a DFT single-point calculation was performed with the BP86 density functional if not mentioned otherwise. For this purpose a Fortran program has been written that automatically carries out all steps for the generation and collection of the raw data. Local spin values were obtained by that program calling our local version of TURBOMOLE's MOLOCH module (employing Löwdin projection operators[33–36,58]). Local spin values smaller than 0.0001 a.u. were set to zero. Broken-symmetry Slater determinants were generated by our restrained optimization tool.[37] It constrains local spins to ideal values[44] and afterwards guides the SCF iterations towards the region with the desired local spin distribution corresponding to an minimum of the energy for the given cluster structure. Finally, structure–property plots were created with the commercially available MATHEMATICA 7.0 program by Wolfram Research.[59]

For the investigation of the transition-state flexibility we implemented a C++ program that distorts a transition-state structure along the pre-selected normal modes to yield distorted structures within a pre-defined energy threshold. The B3LYP/TZVP single-point calculations have been carried out by calls to the TURBOMOLE modules. The vibrational analysis that provides the normal modes has been performed with the SNF program.[60]

Pictures of molecular structures were visualized with PYMOL.[61]

Acknowledgements

This work has been financially supported by the Schweizer Nationalfonds (project no. 200020–121870) and by ETH Zurich (TH Grant 0-20436-07).

References

1 V. K. Yachandra, K. Sauer and M. P. Klein, *Chem. Rev.*, 1996, **96**, 2927–2950.
2 J. P. McEvoy and G. W. Brudvig, *Chem. Rev.*, 2006, **106**, 4455–4483.
3 J. Barber and J. W. Murray, *Coord. Chem. Rev.*, 2008, **252**, 233–243.
4 M. Frey, *ChemBioChem*, 2002, **3**, 153–160.
5 P. M. Vignais and B. Billoud, *Chem. Rev.*, 2007, **107**, 4206–4272.
6 G. J. Leigh. *Nitrogen Fixation at the Millenium*; Elsevier: Amsterdam, 2002.
7 M. Reiher; A. Wolf. *Relativistic Quantum Chemistry. The Fundamental Theory of Molecular Science*; Wiley VCH: Weinheim, 2009.
8 T. Ziegler and J. Autschbach, *Chem. Rev.*, 2005, **105**, 2695–2722.
9 F. Neese, *Coord. Chem. Rev.*, 2009, **253**, 526–563.
10 C. J. Cramer and D. G. Truhlar, *Phys. Chem. Chem. Phys.*, 2009, **11**, 10757.
11 C. J. Cramer. *Essentials of Computational Chemistry: Theories and Models*, 2nd ed.; John Wiley & Sons: New York, 2004.
12 T. Helgaker; P. Jørgensen; J. Olsen *Molecular Electronic-Structure Theory*; John Wiley & Sons: Chichester, England, 2000.
13 K. H. Marti, I. Malkin-Ondik, G. Moritz and M. Reiher, *J. Chem. Phys.*, 2008, **128**, 014104.
14 K. H. Marti, M. Reiher, B. Bauer, M. Troyer and F. Verstraete, *New J. Phys.*, 2010, in press: http://arxiv.org/abs/1004.5303.
15 S. R. White, *Phys. Rev. Lett.*, 1992, **69**, 2863–2866.
16 G. K.-L. Chan; J. J. Dorando; D. Ghosh; J. Hachmann; E. Neuscamman; H. Wang; T. Yanai. In , Frontiers in Quantum Systems in Chemistry and Physics; Prog. Theor. Chem. Phys., Vol. 18; pp 49–65; 12th European Workshop on Quantum Systems in Chemistry and Physics, London, England, AUG 30-SEP 05, 2007.
17 K. H. Marti and M. Reiher, *Z. Phys. Chem.*, 2010, **224**, 583–599.
18 S. Östlund and S. Rommer, *Phys. Rev. Lett.*, 1995, **75**, 3537.
19 S. Rommer and S. Östlund, *Phys. Rev. B: Condens. Matter*, 1997, **55**, 2164–2181.
20 Y. Kurashige and T. Yanai, *J. Chem. Phys.*, 2009, **130**, 234114.
21 A. Sandvik and G. Vidal, *Phys. Rev. Lett.*, 2007, **99**, 220602.
22 F. Verstraete, M. M. Wolf, D. Perez-Garcia and J. I. Cirac, *Phys. Rev. Lett.*, 2006, **96**, 220601.

23 M. Aguado and G. Vidal, *Phys. Chem. Rev.*, 2008, **100**, 070404.
24 C. J. Cramer, M. W loch, P. Piecuch, C. Puzzarini and L. Gagliardi, *J. Phys. Chem. A*, 2006, **110**, 1991–2004.
25 Z. Azizi, B. O. Roos and V. Veryazov, *Phys. Chem. Chem. Phys.*, 2006, **8**, 2727–2732.
26 P. A. Malmqvist, K. Pierloot, A. Rehaman, M. Shahi, C. J. Cramer and L. Gagliardi, *J. Chem. Phys.*, 2008, **128**, 204109.
27 R. M. Dreizler; E. K. U. Gross. *Density Functional Theory — An Approach to the Quantum Many-Body Problem*; Springer-Verlag: Heidelberg, 1990.
28 J. Tao, J. P. Perdew, V. N. Staroverov and G. E. Scuseria, *Phys. Rev. Lett.*, 2003, **91**, 146401.
29 M. Reiher and B. A. Hess, *Chem.–Eur. J.*, 2002, **8**, 5332–5339.
30 O. Einsle, F. A. Tezcan, S. L. A. Andrade, B. Schmid, M. Yoshida, J. B. Howard and D. C. Rees, *Science*, 2002, **297**, 1696–1700.
31 H. M. Senn and W. Thiel, *Angew. Chem., Int. Ed.*, 2009, **48**, 1198–1229.
32 M. Planck, *Das Wesen der Wissenschaft*, stattliches Lautinstitut, Berlin, 1939.
33 A. E. Clark and E. R. Davidson, *J. Chem. Phys.*, 2001, **115**, 7382–7392.
34 C. Herrmann, M. Reiher and B. A. Hess, *J. Chem. Phys.*, 2005, **122**, 034102.
35 M. Podewitz, C. Herrmann, A. Malassa, M. Westerhausen and M. Reiher, *Chem. Phys. Lett.*, 2008, **451**, 301–308.
36 I. Mayer, *Chem. Phys. Lett.*, 2007, **440**, 357–359.
37 C. Herrmann, M. Podewitz and M. Reiher, *Int. J. Quantum Chem.*, 2009, **109**, 2430–2446.
38 K. A. Magnus, H. Tonthat and J. E. Carpenter, *Chem. Rev.*, 1994, **94**, 727–735.
39 E. I. Solomon, F. Tuczek, D. E. Root and C. A. Brown, *Chem. Rev.*, 1994, **94**, 827–856.
40 L. M. Mirica, X. Ottenwaelder and T. D. P. Stack, *Chem. Rev.*, 2004, **104**, 1013–1046.
41 P. E. M. Siegbahn and M. R. A. Blomberg, *Annu. Rev. Phys. Chem.*, 1999, **50**, 221–249.
42 P. E. M. Siegbahn, *Faraday Discuss.*, 2003, **124**, 289–296.
43 B. F. Gherman and C. J. Cramer, *Coord. Chem. Rev.*, 2009, **253**, 723–753.
44 I. Rudra, Q. Wu and T. Van Voorhis, *J. Chem. Phys.*, 2006, **124**, 024103.
45 L. M. Mirica, X. Ottenwaelder and T. D. P. Stack, *Chem. Rev.*, 2004, **104**, 1013–1045.
46 M. Reiher, *Faraday Discuss.*, 2007, **135**, 97–124.
47 X. Yang and M. B. Hall, *J. Am. Chem. Soc.*, 2009, **131**, 10901–10908.
48 L. Jiang, E. A. Althoff, F. R. Clemente, L. Doyle, D. Röthlisberger, A. Zanghellini, J. L. Gallaher, J. L. Betker, F. Tanaka, C. F. Barbas, D. Hilvert, K. N. Houk, B. L. Stoddard and D. Baker, *Science*, 2008, **319**, 1387–1391.
49 D. Röthlisberger, O. Khersonsky, A. M. Wollacott, L. Jiang, J. DeChancie, J. Betker, J. L. Gallaher, E. A. Althoff, A. Zanghellini, O. Dym, S. Albeck, K. N. Houk, D. S. Tawfik and D. Baker, *Nature*, 2008, **453**, 190–195.
50 S. Kozuch and S. Shaik, *J. Am. Chem. Soc.*, 2006, **128**, 3355–3365.
51 S. Kozuch and S. Shaik, *J. Phys. Chem. A*, 2008, **112**, 6032–6041.
52 R. Ahlrichs, M. Bär, M. Häser, H. Horn and C. Kölmel, *Chem. Phys. Lett.*, 1989, **162**, 165–169.
53 A. Schäfer, C. Huber and R. Ahlrichs, *J. Chem. Phys.*, 1994, **100**, 5829–5835.
54 A. D. Becke, *Phys. Rev. A: At., Mol., Opt. Phys.*, 1988, **38**, 3098–3100.
55 J. P. Perdew, *Phys. Rev. B: Condens. Matter*, 1986, **33**, 8822–8824.
56 C. Lee, W. Yang and R. G. Parr, *Phys. Rev. B: Condens. Matter*, 1988, **37**, 785–789.
57 A. D. Becke, *J. Chem. Phys.*, 1993, **98**, 5648–5652.
58 P.-O. Löwdin, *J. Chem. Phys.*, 1950, **18**, 365–375.
59 http://www.wolfram.com/.
60 J. Neugebauer, M. Reiher, C. Kind and B. A. Hess, *J. Comput. Chem.*, 2002, **23**, 895–910.
61 W. L. DeLano. *The PyMOL Molecular Graphics System*; DeLano Scientific: San Carlos, CA, 2002.